

# Regularity and chaos at critical points of first-order quantum phase transitions

M. Macek and A. Leviatan

*Racah Institute of Physics, The Hebrew University, Jerusalem 91904, Israel*

(Dated: April 1, 2024)

We study the interplay between regular and chaotic dynamics at the critical point of a generic first order quantum phase transition in an interacting boson model of nuclei. A classical analysis reveals a distinct behavior of the coexisting phases in a broad energy range. The dynamics is completely regular in the deformed phase and, simultaneously, strongly chaotic in the spherical phase. A quantum analysis of the spectra separates the regular states from the irregular ones, assigns them to particular phases and discloses persisting regular rotational bands in the deformed region.

PACS numbers: 21.60.Fw, 05.45.Mt, 0.5.30.Rt, 21.10.Re

Quantum phase transitions (QPTs) at zero temperature are structural changes of the system's ground state resulting from a variation of parameters  $\lambda$  in the quantum Hamiltonian  $\hat{H}(\lambda)$  [1]. Aspects of QPTs and their finite- $N$  precursors are currently attracting considerable theoretical and experimental interest, as they occur in diverse dynamical systems including spin lattices [2], ensembles of ultracold atoms [3] and atomic nuclei [4].

The particular type of QPT is reflected in the topology of the underlying mean-field (Landau) potential  $V(\lambda)$ . In first order (discontinuous) QPTs,  $V(\lambda)$  develops multiple minima, corresponding to distinct phases (characterized by distinct values of an order parameter) that coexist in a range of  $\lambda$ -values and become degenerate at the critical point  $\lambda = \lambda_c$ . In higher order (continuous) QPTs, the single minimum of  $V(\lambda)$  shifts continuously but non-analytically to a different value of the order parameter at  $\lambda = \lambda_c$ , without phase coexistence.

Interacting many-body systems undergoing QPTs provide a fertile ground for studying the emergence of quantum chaos. A typical example, is the recent analysis in quantum optics models of  $N$  two-level atoms interacting with a single-mode radiation field [5], where the onset of chaos is triggered by continuous QPTs. In this communication, we turn our attention to systems with discontinuous QPTs, where multiple-well potentials and phase coexistence provide even a richer environment to study the interplay of order and chaos. Indeed, studies of 2D single-particle models indicate that the classical motion can be dissimilar (regular or chaotic) in different local minima [6]. In the present work, we show that such mixed form of dynamics and non-uniform onset of chaos arises from rotational-invariant Hamiltonians in a system of  $N$  interacting constituents, undergoing a first-order QPT. A marked separation between regular and chaotic dynamics is observed in both classical and quantum analyses.

As a concrete example, we adopt the interacting boson model (IBM) [7], widely used in the description of quadrupole collective states in nuclei, in terms of a system of  $N$  monopole ( $s$ ) and quadrupole ( $d$ ) bosons, representing valence nucleon pairs. The total boson number  $N$  and angular momentum  $L$  are conserved, which enables to solve the model exactly by numerical diagonalization

of finite matrices for any fixed  $N$  and  $L$ . The model accommodates both continuous and discontinuous quantum shape-phase transitions [8], which are manifested empirically between spherical and deformed nuclei [4].

Apart from kinetic rotational terms, the most general two-body IBM Hamiltonian at the critical point of a first order QPT, can be transcribed in the form [9]

$$\hat{H}_{\text{cri}} = h_2 P_2^\dagger(\beta_0) \cdot \tilde{P}_2(\beta_0) / N(N-1), \quad (1)$$

where  $P_{2\mu}^\dagger(\beta_0) = \beta_0 s^\dagger d_\mu^\dagger + \sqrt{7/2} (d^\dagger d^\dagger)_\mu^{(2)}$ ,  $\tilde{P}_{2\mu}(\beta_0) = (-1)^\mu P_{2,-\mu}(\beta_0)$  and the dot implies a scalar product. To facilitate the comparison with the classical limit, involving large  $N$ , the critical-point Hamiltonian (1) is scaled by  $N(N-1)$ . For  $\beta_0 > 0$ ,  $\hat{H}_{\text{cri}}$  annihilates two distinct degenerate ground states, which have the form of static condensates  $|\beta; N\rangle = (N!)^{-1/2} \Gamma_c^\dagger(\beta)^N |0\rangle$  of  $N$  bosons,  $\Gamma_c^\dagger(\beta) = [\beta d_0^\dagger + \sqrt{2 - \beta^2} s^\dagger] / \sqrt{2}$ , with (i)  $\beta = 0$  (spherical  $s$ -boson condensate) and (ii)  $\beta = \sqrt{2}\beta_0(1 + \beta_0^2)^{-1/2}$  (deformed condensate) and correspond to the two coexisting shape phases of the nucleus. The parameter  $\beta_0$  in  $\hat{H}_{\text{cri}}$  determines the equilibrium deformation in the deformed phase as well as the height of the potential barrier between the two phases (see below).

The classical limit of the IBM is obtained through the use of coherent states [10]. This amounts to replacing  $(s^\dagger, d_\mu^\dagger)$  by six c-numbers  $(\alpha_s^*, \alpha_\mu^*)$  rescaled by  $\sqrt{N}$  and taking  $N \rightarrow \infty$ , with  $1/N$  playing the role of  $\hbar$ . Number conservation ensures that phase space is 10-dimensional and can be phrased in terms of two shape (deformation) variables, three orientation (Euler) angles and their conjugate momenta. Chaotic properties of the IBM have been studied extensively [11], albeit, with a simplified Hamiltonian, giving rise to an extremely low, hence non-generic, barrier. The Hamiltonian of Eq. (1) can accommodate a barrier with an adjustable height, hence allows a systematic study of its impact on the dynamics. In the classical analysis presented below we consider, for simplicity, the dynamics of  $L = 0$  vibrations, for which only two degrees of freedom are active. The rotational dynamics with  $L > 0$  is examined in the subsequent quantum analysis.

For the particular case of the Hamiltonian (1), constrained to  $L = 0$ , the above procedure yields the follow-

ing classical Hamiltonian

$$\begin{aligned} H_{\text{cri}}/h_2 &= \mathcal{H}_{d,0}^2 + p_\gamma^2 + \beta_0^2(1 - \mathcal{H}_{d,0})\mathcal{H}_{d,0} \\ &+ \beta_0\sqrt{(1 - \mathcal{H}_{d,0})/2} \\ &\times [(p_\gamma^2/\beta - \beta p_\beta^2 - \beta^3)\cos 3\gamma + 2p_\beta p_\gamma \sin 3\gamma] . \end{aligned} \quad (2)$$

Here the coordinates  $\beta \in [0, \sqrt{2}]$ ,  $\gamma \in [0, 2\pi)$  and their canonically conjugate momenta  $p_\beta \in [0, \sqrt{2}]$  and  $p_\gamma \in [0, 1]$  span a compact classical phase space. The term  $\mathcal{H}_{d,0} \equiv (T + \beta^2)/2$ , with  $T = p_\beta^2 + p_\gamma^2/\beta^2$ , denotes the classical limit of the  $d$ -boson number operator  $\hat{n}_d = \sum_\mu d_\mu^\dagger d_\mu$  (restricted to  $L = 0$ ) and forms an isotropic harmonic oscillator Hamiltonian in the  $\beta, \gamma$  variables. Notice that (2) contains complicated momentum-dependent terms originating from the two-body interactions in (1), not just the usual quadratic kinetic energy  $T$ . Setting  $p_\beta = p_\gamma = 0$  in Eq. (2) leads to the potential

$$\begin{aligned} V_{\text{cri}}/h_2 &= \frac{1}{2}\beta_0^2\beta^2 + \frac{1}{4}(1 - \beta_0^2)\beta^4 \\ &- \frac{1}{2}\beta_0\sqrt{2 - \beta^2}\beta^3 \cos 3\gamma , \end{aligned} \quad (3)$$

which can be alternatively obtained for  $\gamma = 0$  as an expectation value of  $\hat{H}_{\text{cri}}$  (1) in the static condensate mentioned above,  $V_{\text{cri}}(\beta, \gamma = 0) = \langle \beta; N | \hat{H}_{\text{cri}} | \beta; N \rangle$ . Apart from being compact, the  $\beta, \gamma$  variables are analogous to the coordinates of the geometric collective model [12] and portray the amount of quadrupole deformation ( $\beta = 0$  corresponds to the spherical, while  $\beta > 0$  to deformed shapes) and the triaxiality of the nucleus ( $\gamma = 2\pi k/3$ , with  $k = 0, 1, 2$  correspond to prolate and  $\gamma = \pi/3 + 2\pi k/3$  to oblate axially-symmetric shapes, while other values to triaxial shapes). They may be interpreted as polar coordinates in an abstract plane parametrized by Cartesian coordinates  $x = \beta \cos \gamma$  and  $y = \beta \sin \gamma$ . The potential of Eq. (3) displays a three-fold rotational symmetry about the origin  $\beta = 0$ . Its four minima, being degenerate at energy  $V_{\text{min}} = 0$ , are of two types and correspond to the different phases: (i) the single spherical minimum at  $\beta = 0$  and (ii) the three equivalent deformed minima at  $\beta = \sqrt{2}\beta_0(1 + \beta_0^2)^{-1/2}$  with  $\gamma = 0, 2\pi/3, 4\pi/3$ . In between the spherical and deformed minima, there are three equivalent saddle points located at  $\beta = [1 - (1 + \beta_0^2)^{-1/2}]^{1/2}$ , which create potential barriers of height  $V_b = h_2[1 - (1 + \beta_0^2)^{1/2}]^2/4$ , separating the two phases. The limiting value at the domain boundary is  $V(\beta = \sqrt{2}, \gamma) = h_2$ . The potential of Eq. (3) is similar to that considered in [6], but differs by the square-root term and the compact domain.

The nature of the classical motion associated with the Hamiltonian (2) can be depicted conveniently via Poincaré surfaces of sections in the plane  $y = 0$ , plotting the values of  $x$  and the momentum  $p_x$  each time a trajectory intersects the plane. Regular trajectories are bound to toroidal manifolds within the phase space and their intersections with the plane of section lie on 1D curves (ovals). In contrast, chaotic trajectories randomly cover kinematically accessible areas of the section [13].

Poincaré sections for  $\beta_0 = 1.0, 1.3, 1.5$ , are displayed, respectively, in the left, middle and right columns of Fig. 1. The three cases correspond to “low”, “medium” and “high” potential barriers  $V_b/h_2 = 0.04, 0.10, 0.16$ , (compared to  $V_b/h_2 = 0.0009$  in previous works [11]). In each case (see panels  $a_k$ - $b_k$ - $c_k$ ), we show the sections at five different energies  $E_k$  ( $k=1$ -5) relative to the barrier-tops  $V_b$ :  $E_1 = 0.25V_b$ ,  $E_2 = 0.9V_b$  are below,  $E_3 = V_b$  at, and  $E_4 = 1.1V_b$ ,  $E_5 = 4V_b$  are above the barrier. The bottom row (panels  $a$ - $b$ - $c$ ) depicts the corresponding classical potential  $V_{\text{cri}}(x, y = 0)$ , Eq. (3). In all three cases, the motion is predominantly regular at low energies and gradually turning chaotic as the energy increases. However, the classical dynamics evolves differently in the vicinity of the two wells. The family of regular trajectories near the deformed minimum has a particularly simple structure. It forms a single set of concentric loops around a single stable (elliptic) fixed point. The trajectories remain regular even at energies far exceeding the barrier height  $V_b$ . In contrast, a more complicated structure develops near the spherical minimum. Here, at low energies (panels  $a_1$ - $b_1$ - $c_1$ ), one observes four major islands surrounding stable fixed points, and unstable (hyperbolic) fixed points in-between. As the energy increases (approximately for  $E > V_b/3$  [14]), considerable fraction of the trajectories becomes chaotic (panels  $a_2$ - $b_2$ - $c_2$ ) until complete chaoticity is reached near the barrier top. The clear separation between regular and chaotic dynamics, associated with the two minima, persists all the way to  $E = V_b$ , where the two regions just touch (panels  $a_3$ - $b_3$ - $c_3$ ). At  $E > V_b$ , the chaotic trajectories from the spherical region can penetrate into the deformed region and a layer of chaos develops (panels  $a_4$ - $b_4$ - $c_4$ ), and gradually dominates the surviving regular island for  $E \gg V_b$  (panels  $a_5$ - $b_5$ - $c_5$ ). In general, the regularity is more pronounced for higher barriers (larger  $\beta_0$ ).

Quantum manifestations of classical chaos are often detected by statistical analyses of energy spectra [13]. In a quantum system with mixed regular and irregular states, the statistical properties of the spectrum are usually intermediate between the Poisson and the Gaussian orthogonal ensemble (GOE) statistics. Such global measures of quantum chaos are, however, insufficient to reflect the rich dynamics of an inhomogeneous phase space structure, as in Fig. 1, with well separated regular and chaotic regions. To do so, one needs to distinguish between regular and irregular subsets of eigenstates in the same energy intervals. For that purpose we employ the spectral lattice method of Peres [15], which provides additional properties of individual energy eigenstates. The Peres lattices are constructed by plotting the expectation values  $O_i = \langle i | \hat{O} | i \rangle$  of an arbitrary operator,  $[\hat{O}, \hat{H}] \neq 0$ , versus the energy  $E_i = \langle i | \hat{H} | i \rangle$  of the eigenstates  $|i\rangle$ . The lattices  $\{O_i, E_i\}$  corresponding to regular dynamics can be shown to display a regular pattern, while chaotic dynamics leads to disordered meshes of points. The method has been recently applied to quantum chaos in the geometric collective model of nuclei [16].

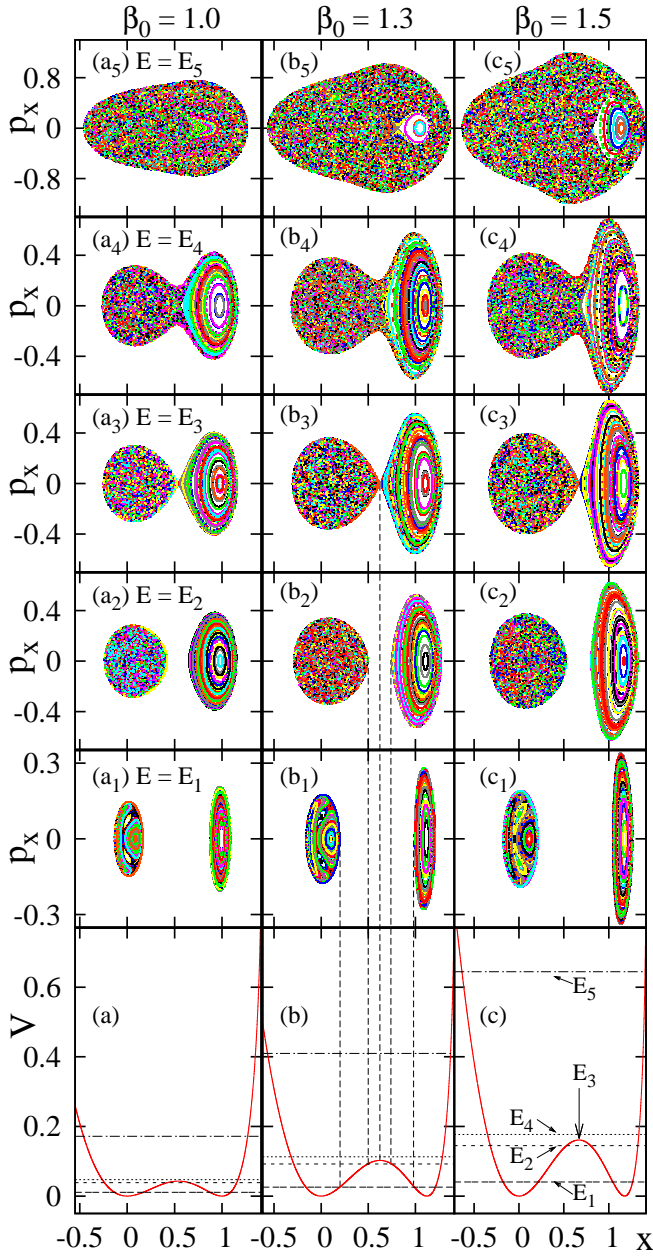


FIG. 1: (Color online). Poincaré sections for the classical Hamiltonian (2) with  $h_2 = 1$  and  $\beta_0 = 1.0, 1.3, 1.5$  (left, middle and right columns, respectively). In each case, the surfaces are drawn at energies  $E_k$  ( $k = 1-5$ ) relative to the barrier-tops  $V_b$ :  $E_1 = 0.25V_b$ ,  $E_2 = 0.9V_b$ ,  $E_3 = V_b$ ,  $E_4 = 1.1V_b$ ,  $E_5 = 4V_b$  (panels  $a_k$ - $b_k$ - $c_k$ ). The bottom row (panels  $a$ - $b$ - $c$ ) depicts the corresponding classical potential  $V_{\text{cri}}(x, y = 0)$ , Eq. (3), with coexisting spherical and deformed minima at  $x = 0$  and  $x \geq 1$ , respectively. The reference energies,  $E_k$ , are indicated by horizontal dashed and dotted lines. Vertical lines mark the turning-points for  $E_k \leq V_b$ . Notice the pronounced separation of regular and chaotic regions in phase space, associated with the two minima.

In the present analysis we choose the Peres operator to be  $\hat{O} = \hat{n}_d$ . The lattices correspond to the set of points

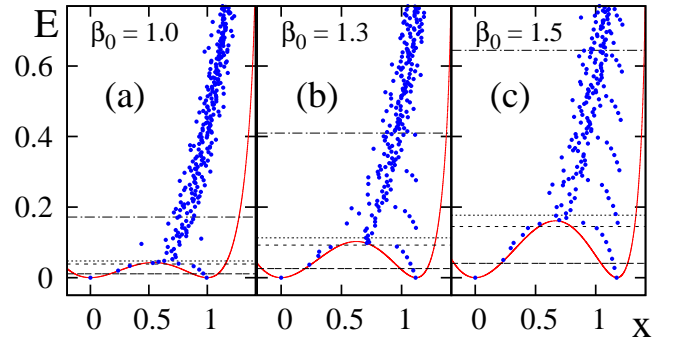


FIG. 2: (Color online). Quantum Peres lattices  $\{x_i, E_i\}$  for  $L = 0$  eigenstates  $|i\rangle$  of  $\hat{H}_{\text{cri}}$  (1), with  $h_2 = 1$ ,  $N = 80$  and  $\beta_0 = 1.0, 1.3, 1.5$ . The quantity  $x_i = \sqrt{2\langle i|\hat{n}_d|i\rangle/N}$  enables a direct comparison with the classical potential  $V_{\text{cri}}(x, y = 0)$ , Eq. (3). The reference energies  $E_1, E_2, E_4, E_5$ , are indicated as in Fig. 1. Notice the sequences of regular states in the deformed region. The lowest sequence consists of  $L = 0$  bandhead states of the ground  $g(K = 0)$  and  $\beta^n(K = 0)$  bands. Regular sequences at higher energy correspond to  $\beta^n\gamma^2(K = 0)$ ,  $\beta^n\gamma^4(K = 0)$  bands, etc.

$\{x_i, E_i\}$ , with  $x_i \equiv \sqrt{2\langle i|\hat{n}_d|i\rangle/N}$  and  $|i\rangle$  being the eigenstates of  $\hat{H}_{\text{cri}}$  (1). The expectation value of  $\hat{n}_d$  in the condensate,  $x = \beta = \sqrt{2\langle \beta; N|\hat{n}_d|\beta; N\rangle/N}$ , is related to the deformation  $\beta$  (whose equilibrium value is the order parameter of the QPT) and the coordinate  $x$  in the classical potential,  $V_{\text{cri}}(x, y = 0) = V_{\text{cri}}(\beta, \gamma = 0)$ , Eq. (3). The spherical ground state has  $n_d = x_i = 0$ . Excited spherical states show characteristic dominance of single  $n_d$  components [9], hence  $x_i \sim \sqrt{n_d/N}$  is small for  $n_d/N \ll 1$ . Rotational members of the deformed ground band are obtained by  $L$ -projection from  $|\beta; N\rangle$  and have  $x_i \approx \beta$  to leading order in  $N$ . This relation is still valid, to a good approximation, for states in excited deformed bands, whose intrinsic states are obtained by replacing condensate bosons in  $|\beta; N\rangle$  with orthogonal bosons representing  $\beta$  and  $\gamma$  excitations [17]. These attributes have the virtue that the lattices  $\{x_i, E_i\}$  can identify the regular/irregular quantum states and associate them with a given region in the classical phase space.

Fig. 2 presents the lattices calculated for  $L = 0$  eigenstates of  $\hat{H}_{\text{cri}}$  with  $N = 80$  and  $\beta_0 = 1.0, 1.3, 1.5$ . In each case, one can clearly identify regular sequences of states localized within and above the respective deformed wells. They form several chains of lattice points close in energy, with the lowest chain originating at the deformed ground state. A close inspection reveals that the  $x_i$ -values of these regular states, lie in the intervals of  $x$ -values occupied by the regular tori in the Poincaré sections in Fig. 1. Similarly to the classical tori, these regular sequences persist to energies well above the barriers  $V_b$ . In contrast, the remaining states, including those residing in the spherical minimum, do not show any obvious patterns and lead to disordered (chaotic) meshes of points at high energy  $E > V_b$ . (Although there are only a few lattice

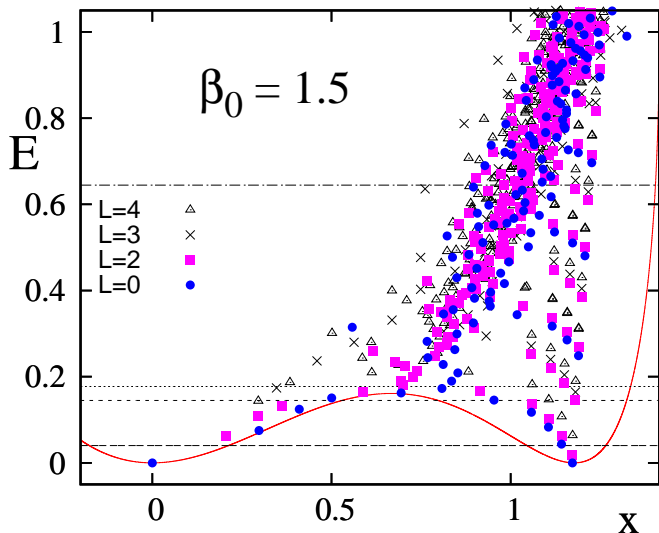


FIG. 3: (Color online). Quantum Peres lattices  $\{x_i, E_i\}$  for eigenstates of  $\hat{H}_{\text{cri}} (1)$  with  $h_2 = 1$ ,  $N = 50$ ,  $\beta_0 = 1.5$  and  $L = 0, 2, 3, 4$ . To enhance visibility, a small  $\hat{L}^2$  term is added, leading to an energy shift  $\Delta E_L = 0.0032L(L+1)$ , without affecting the wave functions. The classical potential  $V_{\text{cri}}(x, y = 0)$  and reference energies  $E_k$  are indicated as in Fig. 2. Notice the rotational bands ( $K = 0, L = 0, 2, 4$ ) and ( $K = 2, L = 2, 3, 4$ ) formed by the regular states in the deformed phase.

points near  $x = 0$ , the chaotic behavior of these spherical states is evident by glancing at the Poincaré sections of Fig. 1). The ability of the Peres method to separate regular states from irregular ones can be tested by fitting the nearest neighbors level spacing distribution of the quantum spectrum by a Brody distribution  $P_\omega(S)$  [13]. The parameter  $\omega$  interpolates between the Poisson ( $\omega = 0$ ) and GOE statistics ( $\omega = 1$ ), corresponding to integrable and fully chaotic classical motion, respectively. We determine  $\omega$  for the full (mixed) spectrum of  $L = 0$  eigenstates and for a partial (“chaotic”) spectrum, from which the tentatively regular levels are excluded. Specifically, for ( $N = 80, \beta_0 = 1.5$ ), we eliminate the 32 levels which form the regular sublattice in the deformed phase (see Fig. 2c) from a set of 364 states with  $E < 0.8$ . For the mixed spectrum we obtain  $\omega = 0.78 \pm 0.10$  and for the “chaotic” spectrum  $\omega = 1.01 \pm 0.10$ , thus confirming the regular character of the excluded levels.

The Peres lattices corresponding to eigenstates of

$\hat{H}_{\text{cri}} (1)$  with  $L = 0, 2, 3, 4$ ,  $N = 50$  and  $\beta_0 = 1.5$  are shown in Fig. 3. They disclose families of regular patterns in the deformed phase. These correspond to rotational bands of states having a common intrinsic structure, as indicated by their nearly equal values of  $\langle \hat{n}_d \rangle$ . The regular  $L = 0$  states form bandheads of rotational sequences  $L = 0, 2, 4, \dots$  ( $K = 0$  bands) and are accompanied by sequences  $L = 2, 3, 4, \dots$  built upon regular  $L = 2$  states ( $K = 2$  bands). Additional  $K$ -bands with  $L = K, K+1, K+2, \dots$  (not shown in Fig. 3) can also be identified. In the nuclear physics terminology, the lowest  $K = 0$  band refers to the ground band and excited  $K$ -bands correspond to multiple  $\beta$  and  $\gamma$  vibrations about the deformed shape with angular momentum projection  $K$  along the symmetry axis. Detailed analysis reveals additional band-like properties of these states, in particular, the coherent decomposition of wave functions in the rotor basis [14]. Such ordered band structures are not present in the chaotic parts of the lattice and their persistence in the spectrum is unexpected, in view of the strong mixing and abrupt structural changes taking place at the critical point. It validates the recently proposed regularity-induced adiabatic separation of intrinsic and collective dynamics [18], for a subset of states.

In summary, we have examined the interplay of regularity and chaos in an interacting system modeling the dynamics at the critical point of a first order QPT between spherical and deformed nuclei. A classical analysis, using Poincaré sections, shows that the two coexisting phases exhibit different susceptibilities towards the onset of chaos. While the deformed phase displays robustly ordered and rather simple dynamics, the spherical phase shows strongly chaotic behavior. An analysis of the quantum spectrum, using Peres lattices, identifies unexpected regular rotational bands in the deformed region, which are absent from the disordered portions of the lattice. Although the regular and chaotic motions coexist in a broad interval of energies, they are well separated and can be distinguished by both classical and quantum calculations. The system in the domain of phase coexistence, thus provides a clear cut demonstration of the classical-quantum correspondence of regular and chaotic behavior, illustrating Percival’s conjecture concerning the distinct properties of regular and irregular quantum spectra [19].

One of us (M.M.) wishes to thank to P. Cejnar for useful discussions. This work is supported by the Israel Science Foundation.

- 
- [1] R. Gilmore and D. H. Feng, Nucl. Phys. A **301**, 189 (1978); R. Gilmore, J. Math. Phys. **20**, 891 (1979).
  - [2] S. Sachdev, *Quantum Phase Transitions* (Cambridge University Press, Cambridge, 1999).
  - [3] M. Greiner, O. Mandel, T. Esslinger, T. W. Hänsch, and I. Bloch, Nature **415**, 39 (2002); K. Baumann, C. Guer-

- lin, F. Brennecke and T. Esslinger, Nature **464**, 1301 (2010).
- [4] P. Cejnar, J. Jolie and R. F. Casten, Rev. Mod. Phys. **82**, 2155 (2010).
- [5] C. Emary and T. Brandes, Phys. Rev. Lett. **90**, 044101 (2003); Phys. Rev. E **67**, 066203 (2003).

- [6] V. P. Berezovoj, Yu. L. Bolotin and V. A. Cherkaskiy, Phys. Lett. A **323**, 218 (2004) and references therein.
- [7] F. Iachello and A. Arima, *The Interacting Boson Model* (Cambridge University Press, Cambridge, 1987).
- [8] A. E. L. Dieperink, O. Scholten and F. Iachello, Phys. Rev. Lett. **44**, 1747 (1980).
- [9] A. Leviatan, Phys. Rev. C **74**, 051301(R) (2006).
- [10] R. L. Hatch and S. Levit, Phys. Rev. C **25**, 614 (1982).
- [11] N. Whelan and Y. Alhassid, Nucl. Phys. A **556**, 42 (1993).
- [12] A. Bohr and B.R. Mottelson, *Nuclear Structure* (World Scientific, Singapore, 1998), Vol. II.
- [13] L. E. Reichl, *The Transition to Chaos in Conservative Classical Systems: Quantum Manifestations* (Springer-Verlag, New York, 1992).
- [14] M. Macek and A. Leviatan, in preparation.
- [15] A. Peres, Phys. Rev. Lett. **53**, 1711 (1984).
- [16] P. Stránský, P. Hruška and P. Cejnar, Phys. Rev. E **79**, 066201 (2009).
- [17] A. Leviatan, Ann. Phys. (NY) **179**, 201 (1987).
- [18] M. Macek, J. Dobeš, P. Stránský and P. Cejnar, Phys. Rev. Lett. **105**, 072503 (2010).
- [19] I. C. Percival, J. Phys. B **6**, L229 (1973).